analytical chemistry

pubs.acs.org/ac Article

Ratiometric Biomimetic Sensor Based on Quantum Dots–Enhanced Glycosylated Carbon Dots for Visual Detection of *Escherichia coli*

Fatemeh Momeni, Saba Ranjbar,* Mohammad Amin Farahmand Nejad, and Mohammad Reza Hormozi-Nezhad

Cite This: *Anal. Chem.* 2026, 98, 818–826 Read Online

ACCESS | Metrics & More | Article Recommendations | Supporting Information

ABSTRACT: We report a fluorescence biomimetic sensor that integrates carbon dots (CDs) and CdTe quantum dots (QDs) for the rapid, antibody-free, and aptamer-free detection of *Escherichia coli O157:H7* (*E. coli O157:H7*) in water samples. This biosensor operates on a ratiometric principle, leveraging green-emitting CDs (GCDs) as a dynamic signal with the red-emitting QDs (RQDs) as a stable reference that significantly enhances the sensor's sensitivity, enabling straightforward visual detection of bacterial contamination. Selectivity was achieved by conjugating mannose—a natural biomimetic receptor— to GCDs, allowing specific recognition of FimH proteins on *E. coli O157:H7*. Upon bacterial binding, the green emission at 508 nm intensifies proportionally to bacterial concentration, while the red fluorescence at 694 nm remains unchanged. This ratiometric biomimetic sensor detects bacterial concentrations ranging from 10^1 to 10^8 CFU/mL within 30 min. The biosensor provides a simple, on-site, naked-eye detection under a portable blue-LED light, with color changes indicating water safety status: green for high bacterial loads, yellow/orange for moderate contamination, and red for safe water. It was successfully applied to tap water, bottled mineral water, surface and groundwater, as well as to samples collected at multiple stages of water treatment plants (12 sources; five replicates). Comprehensive characterization of the nanomaterials was performed using Fourier-transform infrared spectroscopy (FTIR), UV–vis absorption, fluorescence spectroscopy, transmission electron microscopy (TEM), dynamic light scattering (DLS), and zeta potential analysis. This portable, cost-effective biomimetic sensor provides a rapid, reliable alternative to conventional microbiological methods for monitoring drinking water.

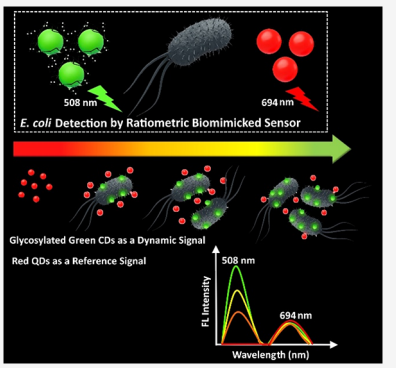

INTRODUCTION

Escherichia coli (*E. coli*) is a common Gram-negative bacterium that normally inhabits the intestines of humans and animals. While most strains are harmless, pathogenic variants like *E. coli O157:H7* produce Shiga toxins, leading to severe illnesses.[1,2] Contamination of water sources with *E. coli O157:H7* is a major pathway for infection, causing diarrheal diseases that are among the world's leading causes of death, particularly in children under five. The World Health Organization (WHO) recommends zero detectable *E. coli O157:H7* in 100 mL of drinking water to ensure safety. Despite these standards, over a billion people still lack access to safe water, resulting in over 2.2 million annual deaths from waterborne illnesses linked to poor sanitation.[3,4] Its low infectious dose and ability to survive in soil, water, and food highlight the urgent need for effective detection methods to protect public health, especially in resource-limited regions.[5]

Conventional methods for detecting *E. coli O157:H7* primarily include culture-based techniques, Polymerase Chain Reaction (PCR), and Enzyme-Linked Immunosorbent Assay (ELISA). Culture methods, which involve growing bacteria on nutrient media and counting colonies, are considered highly reliable across various sample types such as food and water. However, they are time-consuming, often taking over 16–24 h, and require specialized procedures. PCR and its advanced variants, especially real-time PCR, offer rapid and specific detection by amplifying bacterial DNA, while ELISA detects bacteria through antigen–antibody interactions.[6] Despite their advantages, these methods are costly, require skilled personnel, sophisticated equipment, and complex protocols, which limit their practicality in urgent situations or resource-limited settings.[7]

To overcome these challenges, sensor-based approaches targeting *E. coli O157:H7* using appropriate materials have attracted considerable attention. These methods are affordable, easy to use, rapid, and portable, making them especially valuable during public health emergencies and in areas lacking laboratory infrastructure.[8] Among various sensing materials, fluorescence-based sensors stand out due to their high

Received: September 26, 2025
Revised: December 13, 2025
Accepted: December 23, 2025
Published: December 31, 2025

https://doi.org/10.1021/acs.analchem.5c06000
Anal. Chem. 2026, 98, 818–826

sensitivity, minimal equipment requirements (such as a UV lamp), and compatibility with mobile devices for straightforward data collection and analysis.[9,10] Fluorescent dyes were among the first candidates employed for bacterial labeling and real-time detection; however, their use is limited by toxicity, poor photostability, high costs, photodegradation, and lack of specificity, which restrict experimental duration and resolution. As a promising alternative, fluorescent nanomaterials functionalized with specific recognition elements such as aptamers, antibodies, bacteriophages, carbohydrates, and antimicrobial peptides offer effective solutions for bacterial labeling and sensing, overcoming many limitations of traditional dyes.[11]

Carbon dots (CDs) provide tunable fluorescence, low toxicity, and ease of handling and are attractive alternatives to conventional fluorescent probes. More photostable than organic dyes and eliminating the need for genetic modification required by fluorescent proteins, CDs also benefit from straightforward, scalable production and functionalization. Prepared by bottom-up methods (hydrothermal, solvothermal, microwave, pyrolysis) from abundant carbon or biomass precursors, these routes use mild conditions, avoid hazardous reagents, give high yields, and allow scale-up. Because they are typically metal-free or only lightly doped, CDs exhibit low cytotoxicity, good biocompatibility, and colloidal stability in biological media, enhancing their suitability for in vitro and in vivo cell-tracking applications.[12,13]

Their optical properties are tuned by precursor, size, core structure, heteroatom doping, surface passivation and conjugation, achieving broad excitation/emission and high quantum yields for imaging. CDs present abundant surface functional groups (carboxyl, hydroxyl, and amine) that support a wide range of modification strategies. Ligands such as antibodies, peptides, aptamers, small molecules, and polymers can be grafted through covalent bonding (EDC/NHS, silanization, click) or assembled via noncovalent interactions (electrostatic adsorption, $\pi-\pi$ stacking, hydrophobic interactions). These combined features make CDs well suited for cell tracking, allowing precise detection and discrimination of different cell types or microbial strains, capabilities that are vital for medical diagnostics, environmental monitoring, and food safety.[14,15]

Naturally inspired carbohydrate-based receptors are promising for engineering CDs for selective cell adhesion and targeting due to their cost-effectiveness, stability, and essential biological functions. The mammalian cell surface is enveloped by the glycocalyx, a dense carbohydrate layer that many pathogens exploit via specific surface proteins to initiate infection.[16] This intrinsic affinity enables strong and rapid binding interactions that can be exploited for diagnostic applications.[17] For instance, the bacterial protein FimH on *E. coli O157:H7* fimbriae binds selectively to mannose, enabling targeted detection. In our earlier work,[18] density functional theory (DFT) calculations using an alchemical thermodynamic cycle yielded a mannose−FimH binding free energy of about −11 kcal·mol^{-1}.This result agrees with earlier theoretical reports of ΔG = −12.98 kcal·mol^{-1},[19] supporting mannose's strong affinity for *E. coli*. Complementary experimental validation by Li et al.[20] employed competitive binding assays with saccharides and confirmed mannose's markedly higher capture efficiency versus glucose, fructose, sucrose, and lactose.

Glycosylated CDs that mimic these mannose presentations, serving as biomimetic tools, have shown potential for quick and reliable labeling and sensing of *E. coli O157:H7*. However, despite these advantages, research in this area remains limited.[21,22] This limitation arises from the relatively low sensitivity of mannose-bacteria interactions at low concentrations, which hampers effective detection and visual identification. Therefore, further efforts are needed to enhance detection sensitivity and develop more accurate pathogen identification methods.

The ratiometric approach significantly enhances the sensitivity and reliability of fluorescence sensors by utilizing at least two distinct emissive reporters that respond differently to the target analyte.[23] In some designs, one fluorescent reporter dynamically changes in response to analyte concentration, while the second fluorescent reporter serves as an internal reference and remains essentially constant. In other designs, both fluorescent reporters shift upon interaction with the analyte. By taking the ratio of the two fluorescence intensities instead of relying on a single absolute intensity, the system self-calibrates and inherently compensates for common sources of error, such as variations in excitation intensity, photobleaching, probe concentration, optical alignment, and instrument variability.[24,25]

This internal calibration also mitigates the impact of sample-specific matrix effects (e.g., background fluorescence or absorbance), resulting in more accurate and repeatable analytical signals compared to single-intensity methods. In the context of visual detection, ratiometric dual-emission readouts offer clear practical advantages. Dual-color outputs produce noticeable hue shifts that are easier for the naked eye to distinguish than subtle intensity changes, enabling rapid semiquantitative on-site screening without the need for sophisticated instruments. Additionally, these results can be further quantified using smartphones or simple camera-based RGB analysis. By combining fluorescent nanomaterials, researchers can exploit their complementary optical properties to improve biosensor versatility and reliability, especially in complex analytical environments.

In this study we present a ratiometric, tube-based assay for rapid, instrument-free detection of *E. coli O157:H7*. This assay combines red-emitting cadmium telluride quantum dots (CdTe RQDs) as a stable reference with glycosylated, green-emitting carbon dots (GCDs) that act as concentration-responsive labels, intensifying with increasing bacterial binding. Their complementary emissions span a wide range from green through yellow, orange and red enabling naked-eye readout and smartphone RGB quantification without the need for spectrophotometers or fluorescence microscopes. CdTe QDs offer several desirable optical properties: high quantum yields, producing very bright fluorescence, and excellent photostability, which minimizes photobleaching during prolonged illumination. Their emission is both narrow and size-tunable—by controlling their size during synthesis. Importantly, by combining this ratiometric strategy with a biomimetic mannose receptor that targets the FimH adhesin of *E. coli O157:H7*, the platform operates without antibodies or aptamers, yielding a simple, low-cost, and highly accessible detection method.

EXPERIMENTAL SECTION

Synthesis of Fluorescent Probes

The GCDs and CdTe RQDs were synthesized according to previous reports.[26,27] Detailed synthesis procedures can be found in the Supporting Information.

https://doi.org/10.1021/acs.analchem.5c06000
Anal. Chem. 2026, 98, 818−826

Scheme 1. Schematic Illustration of the Synthesis of GCDs and Their Conjugation with Mannose, Synthesis of RQDs, and the Dual-Emission Sensing Strategy Using Man-GCDs as the Label and RQDs as the Reference Signal.

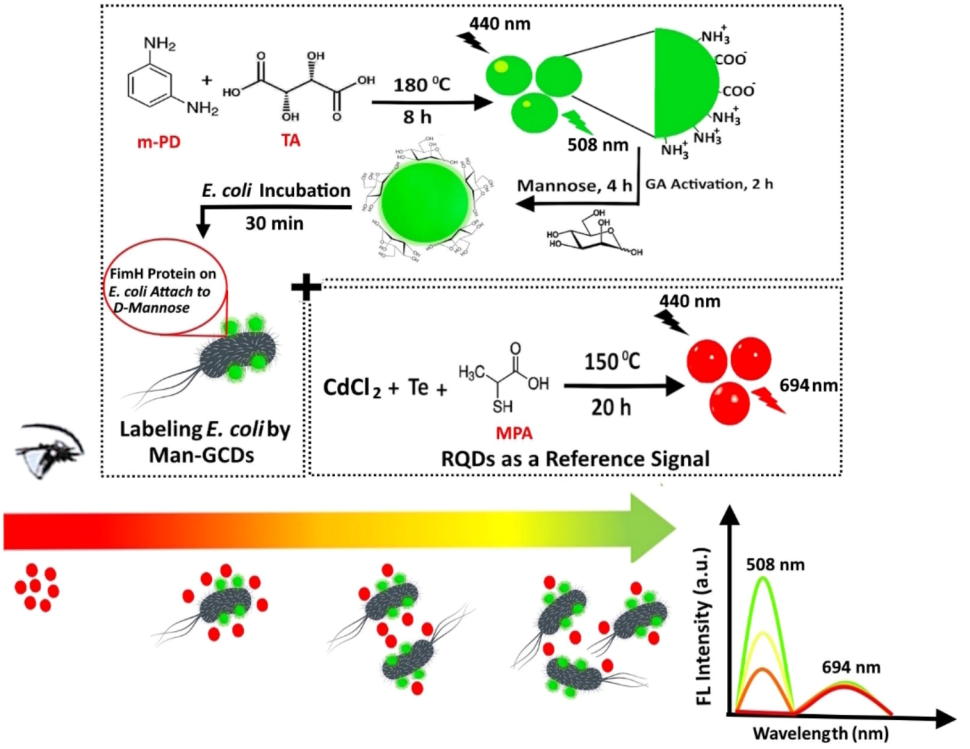

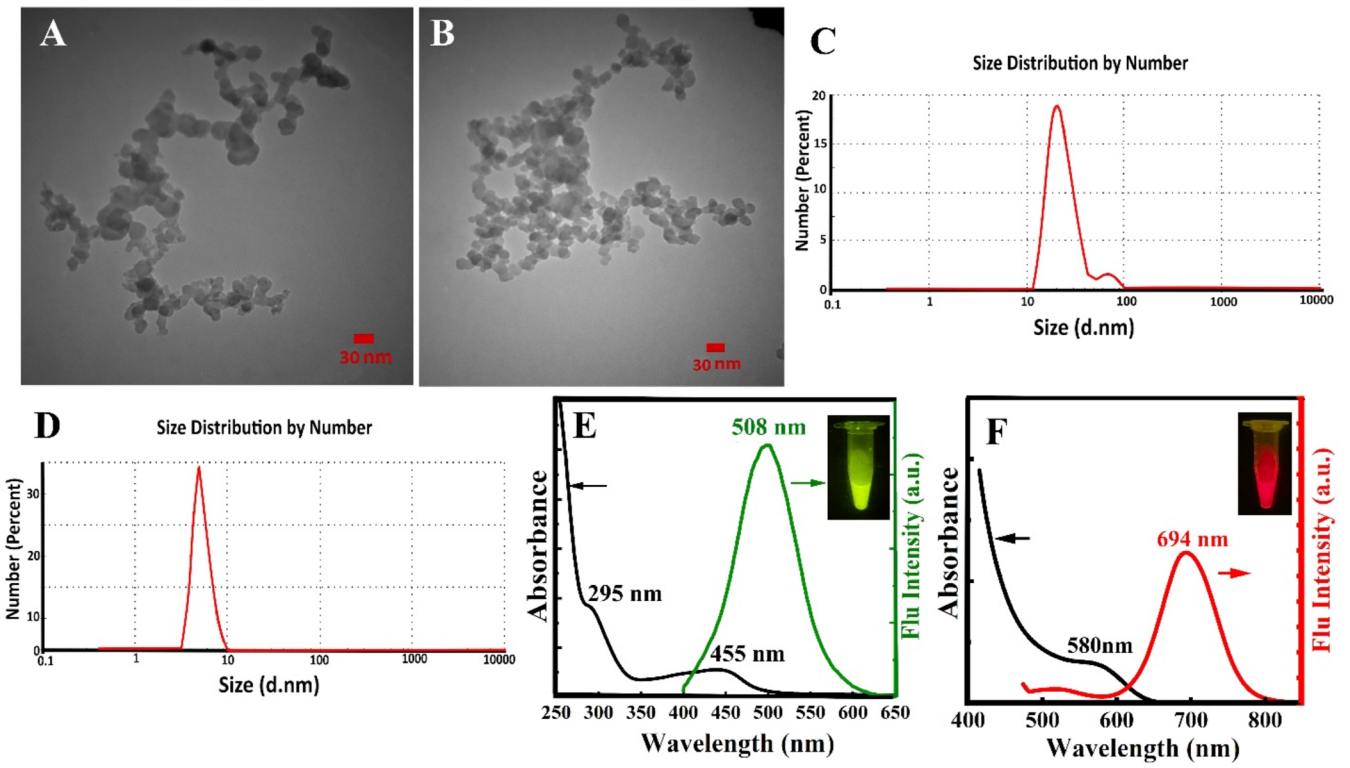

Figure 1. TEM images of (A) GCDs and (B) RQDs; DLS analysis of (C) GCDs and (D) RQDs; UV−vis absorption spectra and fluorescence emission spectra of (E) GCDs and (F) RQDs excited at 440 nm.

Labeling of GCDs with Mannose and Antibody

Mannose was attached to GCDs via a glutaraldehyde-mediated cross-linking process. First, 5.0 mL of GCD solution (1.0 mg/mL) was activated with 500 μL of 2.5% glutaraldehyde (GA) and incubated for 2 h in stirring, dark conditions. Then, 50.0 mg of mannose was added and the mixture incubated for an additional 4 h to form Man-GCDs. Unreacted GA and excess mannose diffused out during dialysis against deionized water

https://doi.org/10.1021/acs.analchem.5c06000
Anal. Chem. 2026, 98, 818−826

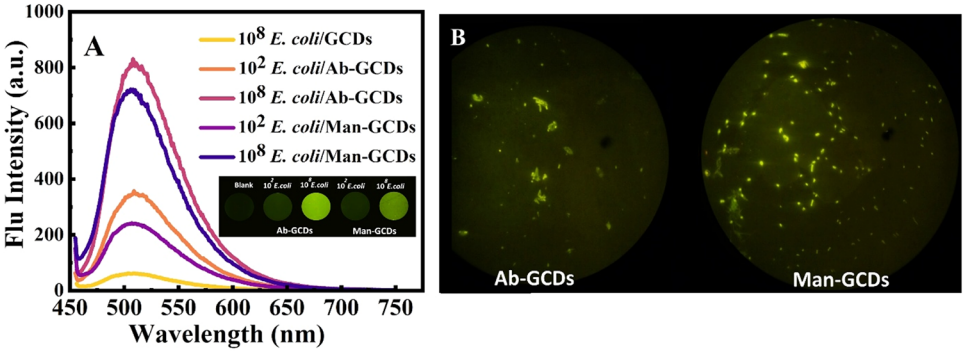

Figure 2. (A) Fluorescence spectra and images captured under excitation at 440 nm; (B) fluorescence microscopy images illustrating the binding of mannose and antibody to *E. coli O157:H7*.

using a 3 kDa membrane with three water exchanges over 12 h, while Man-GCDs were retained inside the dialysis bag. The experiment was repeated with varying mannose amounts (15, 25, and 100 mg) to optimize the mannose-to-GCD ratio.

For comparison, polyclonal antibodies targeting *E. coli O157:H7* were conjugated to GCDs using a similar method. Specifically, 500 μL of polyclonal O/K antibody (0.25 mg/mL) was added to 5.0 mL of GCDs (1.0 mg/mL), activated with 500 μL of 2.5% GA, and incubated for 4 h. The resulting Ab-GCDs label were purified via dialysis. This setup allowed assessment of mannose effectiveness versus antibody, as a standard receptor, in capturing *E. coli O157:H7*.

Fluorescent Labels Assembly and Dual-Emission Strategy

First, 250 μL of *E. coli O157:H7* suspension at a known concentration were mixed with an equal volume of synthesized Man-GCDs. The mixture was then incubated for 30 min under shaking, allowing the bacterial protein FimH to bind to the mannose groups on the GCDs, promoting bacterial attachment and labeling to visualization. After incubation, samples were centrifuged at 7400*g* for 20 min to separate Man-GCD−bound *E. coli* from unbound Man-GCDs. The resulting pellet was resuspended in a tube containing 500 μL of PBS involve 15 μL of RQDs (optimized conditions), which served as a reference signal or contrasting agent. Emissions at 508 and 694 nm were recorded, and the fluorescence intensity ratio of Man-GCDs to RQDs (F_{508}/F_{694}) was used as the measurement signal and plotted against *E. coli O157:H7* concentration. During the lab-on-a-tube sensing procedure, higher concentrations of *E. coli* resulted in increased signals from Man-GCDs, due to greater FimH protein expression and labeling on mannose-conjugated GCDs. Meanwhile, the RQDs served as a stable contrast agent or reference signal, maintaining constant regardless of bacterial concentration. The schematic representation of the nano fluorescents synthesis and sensing strategy is shown in Scheme 1.

All samples were carefully mixed prior to recording the fluorescence spectra and capturing images, with excitation at 440 nm and both excitation and emission slit widths set to 10 nm. This process was repeated across bacterial concentrations ranging from 10^1 to 10^8 CFU/mL, with five replicates at each concentration to ensure reliable calibration of the sensor.

RESULTS AND DISCUSSION

Preliminary Investigation

The fluorescent nanomaterials used in this study were thoroughly prepared and characterized by several complementary techniques. TEM images demonstrated that both GCDs and RQDs are distinct spherical with a relatively uniform size distribution—around 10 nm for both types—in agreement with prior reports.[28,29] (Figure 1A,B). As shown in Figure 1C, DLS analysis revealed hydrodynamic diameter of ∼20 nm for GCDs larger than the TEM size due to the solvation layer surrounding the particles in solution. The GCDs exhibited a zeta potential of approximately +20.2 mV, indicating high colloidal stability in PBS at pH 7.4 (Figure S1), likely due to amine protonation.[30] The RQDs also exhibited an average diameter of ∼6 nm and a zeta potential around −8.9 mV, attributable to deprotonated carboxylate groups from the MPA coating at pH 7.4[31] as shown in Figures 1D and S1.

The spectra in Figure 1E show that GCDs synthesized from m-PD/TA precursors have a strong absorption peak at 295 nm, corresponding to $\pi-\pi^*$ transitions within the benzene-like carbon core, and a secondary peak at 455 nm arising from surface-oxidation−related $n-\pi^*$ transitions involving C═N and C═O groups. Upon 440 nm excitation, these CDs fluoresce at 508 nm, emitting green light in PBS at pH 7.4. Their emission intensity and wavelength are influenced by the size of the core's sp^2 domains and by surface defects related to C═O and C═N functionalities.[32] Similarly, the absorption and emission spectra of CdTe QDs (Figure 1F) reveal a maximum absorption at 580 nm, marking the band-edge excitonic transition, which indicates photon absorption that promotes an electron from the valence band to the conduction band to form an exciton. The peak emission at 694 nm (under 440 nm excitation) confirms the characteristic red fluorescence of CdTe QDs.[27]

The chemical structure, functional groups, and conjugation of GCDs to mannose were analyzed by FT-IR spectroscopy (Figure S2). The GCDs exhibit characteristic bands including aromatic C−H out-of-plane bending at 770 cm^{-1}, C−N stretching vibrations typical of aromatic amines at 1010 cm^{-1}, C−O stretching at 1210 cm^{-1}, C−N stretching along with possible N−H bending in amines at 1440 cm^{-1}, C═N/C═C stretching at 1610 cm^{-1}, C═O stretching at 1730 cm^{-1}, symmetric C−H stretching at 2940 cm^{-1}, and N−H stretching of $-NH_2$ along with O−H stretching of −COOH groups near 3450 cm^{-1} confirming the presence of amino groups ($-NH_2$).[33] Mannose displays peaks at 1368 cm^{-1} (C−H bending in methyl/methylene groups), 1652 cm^{-1} (C═O stretching of carbonyls), 2929 cm^{-1} (symmetric C−H stretching of the cyclopentane ring), and 3419 cm^{-1} (O−H stretching of hydroxyls). Upon conjugation, the intensity of the $-NH_2$ peak declines and its band shifts to ∼3415 cm^{-1},

https://doi.org/10.1021/acs.analchem.5c06000
Anal. Chem. 2026, 98, 818−826

suggesting involvement of amino groups in bonding to mannose. Additionally, the C−N band shifts from 1440 to ∼1384 cm^{-1}, supporting covalent linkage between GCDs and mannose, likely via reaction of GCD amino groups with mannose hydroxyls.[26]

To assess mannose's role in sensing *E. coli O157:H7*, 10^8 CFU/mL were incubated with GCDs (as a blank). The results indicated that, in the absence of mannose in the sensor, GCD binding to the bacteria was weak and driven primarily by electrostatic attraction between the positively charged CDs and the negatively charged bacterial cell wall; this weak association was removed during the washing steps. Moreover, the performance of mannose specifically binds to *E. coli* FimH proteins, was compared with that of standard receptors such as polyclonal antibodies. Results show that the mannose-based label (Man-GCDs) achieves about 80% of the sensitivity of the antibody-based label (Ab-GCDs) for detecting *E. coli O157:H7* at 10^8 and 10^2 CFU/mL. This comparable performance is noteworthy because, despite its slightly lower sensitivity, mannose offers a substantial cost advantage in biosensor construction. Fluorescence spectroscopy, microscopy imaging, and blue-LED irradiation clearly confirmed successful bacterial labeling with both Ab-GCDs and Man-GCDs, as *E. coli O157:H7* attached to both receptors (Figure 2A,B).

Optimization of Experimental Parameters

To achieve precise and sensitive detection of *E. coli O157:H7*, key parameters influencing the sensor's response systematically were optimized before testing. This included buffer pH, the mannose-to-GCDs ratio, the construction of the fluorescent label, the volume ratio of Man-GCDs to *E. coli O157:H7*, incubation time, and the ratio of RQDs to Man-GCDs.

First, the fluorescence intensity of Man-GCDs was assessed at pH levels 4.0, 7.4, and 9.0. Fluorescence spectra with 440 nm excitation and images taken under blue LED illumination, indicated that emission was stronger in acidic and neutral conditions compared to alkaline ones. No notable difference was observed between pH 4.0 and pH 7.4. Based on these findings, subsequent measurements were conducted in a neutral environment using PBS at pH 7.4 (Figure S3).

The optimal mannose loading on the fluorescent label was determined by maintaining a constant concentration of GCDs (5 mL of 1 mg/mL) and adding varying quantities of mannose—15, 25, 50, and 100 mg—to capture bacteria in concentrations of 10^2 CFU/mL and 10^8 CFU/mL. The findings revealed that at the higher bacterial concentration (10^8 CFU/mL), the fluorescence emission at 508 nm remained steady across all mannose concentrations, due to the sufficient number of bacteria present in the sample. In contrast, at the lower bacterial load (10^2 CFU/mL), increasing mannose from 15 to 50 mg enhanced the binding of Man-GCDs to the bacteria, likely due to the increased availability of binding sites on the *E. coli* FimH protein. However, beyond 50 mg, further glycosylation of GCDs resulted in a decrease in fluorescence intensity. This decline is attributed to excessive mannose on the GCD surface, leading to aggregation and hindering effective interaction between mannose and FimH, thereby reducing binding efficiency (Figure S4). Therefore, the optimal loading was set to 50 mg of mannose per 5 mg of GCDs for label preparation.

Next, we optimized the bacteria to label ratio by testing volume ratios of 1:3, 1:1, and 3:1 for *E. coli O157:H7* to Man-GCDs at concentrations of 10^2 CFU/mL and 10^8 CFU/mL, with a total volume of 500 μL. The findings, shown in Figure S5, indicate that the highest sensor response occurs at a 1:1 ratio—250 μL of the label combined with 250 μL of bacterial suspension—where the maximum emission was observed at 508 nm. A small number of Man-GCDs results in fewer labeled bacteria and a weaker signal. Conversely, an excess of Man-GCDs with low bacterial content leaves many unbound fluorescent labels that are washed away during sample processing, also leading to a weak signal.

To optimize incubation conditions, *E. coli O157:H7* suspensions at 10^2 and 10^8 CFU/mL were incubated for 15, 30, and 45 min, and fluorescence was measured at 508 nm. At the high concentration (10^8 CFU/mL), fluorescence remained essentially constant across all time points, indicating rapid and complete labeling. At the lower concentration (10^2 CFU/mL), fluorescence increased with time and peaked at 30 min, after which no significant gain was observed. These results identify 30 min as the optimal incubation time for effective mannose binding to *E. coli O157:H7* FimH (Figure S6).

So far, *E. coli O157:H7* detection has primarily relied on fluorescent tagging with glycosylated GCDs. Moving forward, we propose a ratiometric sensing strategy to enable straightforward visual detection, suitable for laboratories with limited resources. In our design, a biomimetic sensor incorporates RQDs as reference signals by adding 15, 25, or 50 μL of CdTe QDs to PBS. These RQDs serve as contrasting agents or reference signal to enhance the visualization of bacteria labeled with green-emitting Man-GCDs. The choice of red-emitting QDs was strategic, as their emission, combined with the green fluorescence from GCDs, produces a more vivid and distinguishable color spectrum—ranging from green to yellow, orange, and red—depending on their volumetric ratios.

We tested control samples without bacteria, as well as samples containing 10^2, 10^4, and 10^8 CFU/mL of *E. coli O157:H7*. In the absence of RQDs, all the bacteria suspensions exhibited only green fluorescence, which made visual discrimination challenging at low concentrations. When 25 and 50 μL of RQDs were added, the labeled bacteria rapidly shifted to orange or red, indicating the dominant red emission from the QDs over the green bacterial signal. However, these conditions produced primarily red/orange colors, which are not ideal for straightforward visual detection. The best contrast was achieved with 15 μL of RQDs, yielding the most distinct color differences across bacterial concentrations. The control sample without bacteria remained entirely red, confirming the absence of green-labeled bacteria. At the lowest bacterial density (10^2 CFU/mL), the emission appeared orange, while higher densities produced a shift toward yellow and green hues. Notably, at the highest concentration (10^8 CFU/mL), green fluorescence was clearly visible (Figure 3A−D). All experiments were performed in triplicate to ensure consistency and reliability of these observations.

Dual-Emission Sensing of *E. coli* O157:H7

After thoroughly characterizing the biosensor and optimizing the experimental conditions, its ability to detect varying concentrations of *E. coli O157:H7* was assessed. Initially, single-wavelength measurements were focused on the emission of Man-GCDs at 508 nm (F_{508}), which results from mannose binding to *E. coli O157:H7* FimH proteins, across bacterial concentrations ranging from 10^1 to 10^8 CFU/mL (Figure 4A). Although the bacterial presence causes a visible green fluorescence in the tube, easily noticeable by the naked eye,

https://doi.org/10.1021/acs.analchem.5c06000
Anal. Chem. 2026, 98, 818−826

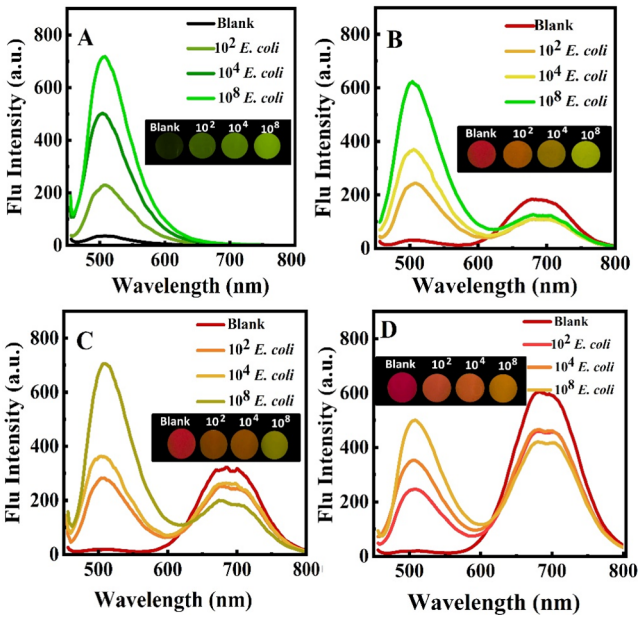

Figure 3. Optimization of RQDs amount for constructing the ratiometric biosensor targeting *E. coli O157:H7* concentrations of 10^2, 10^4, and 10^8 CFU/mL. Fluorescence spectra and recorded images under blue light (440 nm) are shown for different RQD volumes: (A) 0 μL, (B) 15 μL, (C) 25 μL, and (D) 50 μL. The biosensor was incubated for 30 min at pH 7.4.

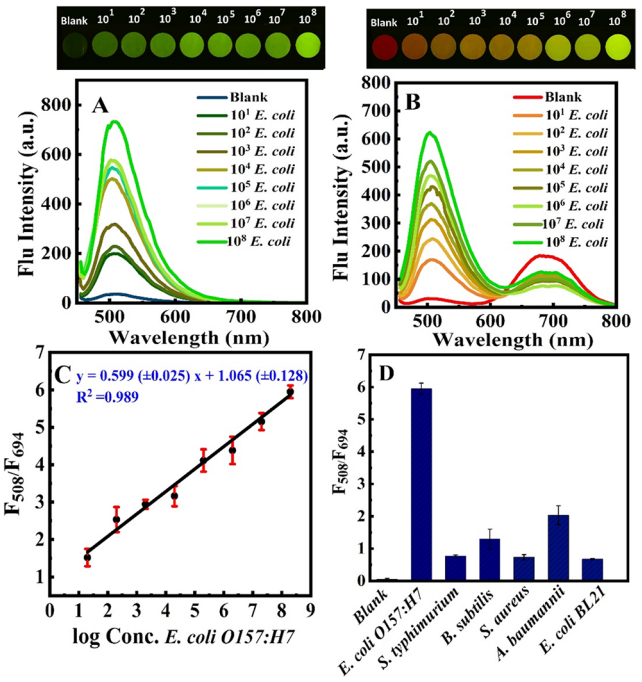

Figure 4. Fluorescence spectra and images recorded under 440 nm excitation for (A) Man-GCDs detecting *E. coli O157:H7* with a single emission at 508 nm; (B) Man-GCDs combined with RQDs for ratiometric detection of *E. coli O157:H7*, showing dual emissions at 508 and 694 nm; (C) calibration curve of the ratiometric biosensor, plotting the ratio of emissions at 508 to 694 nm versus the logarithm of *E. coli O157:H7* concentration; (D) selectivity of the sensor response to *E. coli O157:H7* compared to other bacteria.

distinguishing different bacterial concentrations visually or spectrally proved challenging at this stage. Specifically, it was difficult to differentiate between concentrations such as 10^1 and 10^2 CFU/mL, or between 10^5, 10^6 and 10^7 CFU/mL, based on fluorescence intensity at 508 nm.

To overcome this limitation, a reference signal was introduced by adding 15 μL of RQDs (optimized value) to the tube, enhancing visual contrast and improving detection. This adjustment significantly improved both the spectral and optical differentiation (Figure 4B). The analytical signal was then defined as the ratio of the Man-GCDs emission at 508 nm to the RQDs emission at 694 nm (F_{508}/F_{694}). Since the green emission increases with higher bacterial concentrations while the red emission remains constant, the ratio exhibits an ascending trend. As shown in Figure 4C, there is a linear correlation between the fluorescence intensity ratio and the logarithm of *E. coli O157:H7* concentration within the range of 10^1 to 10^8 CFU/mL. The sensor's limit of quantification (LOQ) was determined to be 10 CFU/mL, with calibration curves generated from five replicate measurements. The photographs captured with a smartphone were further analyzed using RGB Color Detector software to extract RGB data. Since the GCD was employed as the dynamic signal and RQD served as the reference, we utilized the G and R channels to quantify the images. The results (Figure S7) demonstrate a strong correlation between the G/R ratio and the logarithm of *E. coli O157:H7* concentration, highlighting the instrument-free nature and effectiveness of the developed sensing strategy for *E. coli O157:H7* detection.

Repeatability was evaluated by performing five replicate measurements of F_{508}/F_{694} for the blank and each concentration of *E. coli O157:H7*. The resulting relative standard deviations (RSDs) ranged from 2.3% to 12.2%, indicating good repeatability and precision for the proposed sensor.

The selectivity of the biomimetic sensor was evaluated by comparing its response to *E. coli O157:H7* and five other bacteria (*Salmonella typhimurium*, *Acinetobacter baumannii*, *Staphylococcus aureus*, *Bacillus subtilis*, and *E. coli BL21*) by monitoring the F_{508}/F_{694} ratio at 10^8 CFU/mL (Figure 4D). The sensor produced a markedly stronger signal for *E. coli O157:H7*, which expresses higher levels of FimH on its surface. Although, *A. baumannii* expresses type 1 pili with the FimH,[34] its fluorescence response differed substantially from that of *E. coli O157:H7*. These results demonstrate that this assay can distinguish bacterial strains that express different level of FimH protein. The responses recorded for other bacteria are attributable to nonspecific effects, including surface adsorption or entrapment of GCDs within aggregates or extracellular matrix, which is different from specific FimH−mannose interactions in *E. coli O157:H7*.

The stability of the biosensor components (Man-GCDs and RQDs) was evaluated under various conditions. For temperature stability, samples were stored at 4 °C (refrigerator), 25 °C (room temperature), and 37 °C (incubator) and their fluorescence spectra were recorded with identical instrument settings over a one-week. Neither nanomaterial showed a significant loss of emission intensity or a shift in emission peak at any tested temperature (Figure S8). Photostability was assessed by continuous illumination at 440 nm for 1 h. Man-GCDs exhibited excellent photostability, with only minimal photobleaching (less than 10%) and no discernible change in spectral profile after exposure. Even after 3 h, a stable state was still observed. RQDs showed a slightly higher fluorescence decay (around 23%) but remained acceptably stable under these conditions (Figure S9). Long-term stability was

https://doi.org/10.1021/acs.analchem.5c06000
Anal. Chem. 2026, 98, 818−826

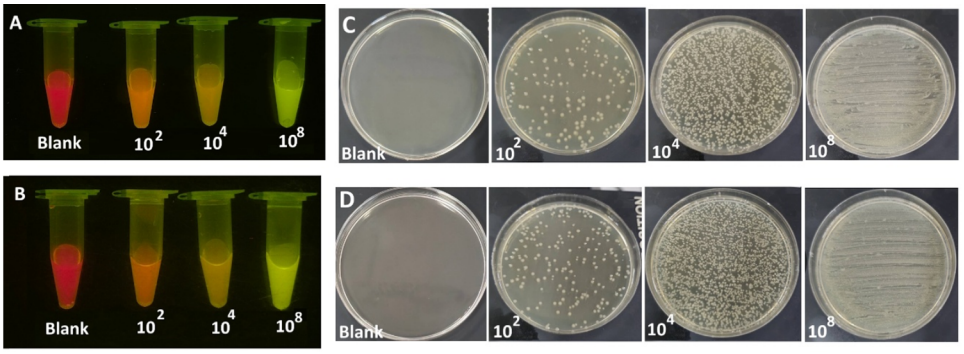

Figure 5. Visual detection results of *E. coli O157:H7* contamination in collected and spiked real samples: (A) tap water and (B) mineral water with varying concentrations of *E. coli O157:H7*; and (C, D) corresponding results obtained using the standard plate culture method.

evaluated over six months with samples stored in the dark at room temperature. Fluorescence spectra and images obtained under 440 nm excitation revealed no significant reduction in intensity for either Man-GCDs or RQDs, indicating excellent long-term stability (Figure S10).

To evaluate the performance of the proposed ratiometric sensor, we compared it with several recently developed optical biosensors that utilize CDs and mannose, as summarized in Table S1. Studies show that CDs can be conjugated to a variety of receptors, including antibodies,[35,36] aptamers,[37,38] and mannose,[21,22] for the detection of *E. coli*. Among these, antibodies offer the highest selectivity and minimize the false positive errors. However, in terms of cost and stability in different environment, mannose and aptamers demonstrate superior performance. In particular, mannose combined with other nanomaterials forms effective bioinspired probes capable of detecting *E. coli* across a broad concentration range.[20,39,40] Notably, the sensor developed in this study leverages a ratiometric approach with biomimetic receptor that enables visual detection without a fluorescence spectrophotometer, while achieving a wide linear range and a low detection limit. This capability represents a significant advantage, especially in resource-limited settings. Table S1 also includes several commercial *E. coli* detection kits, which serve as practical benchmarks for sensitivity, selectivity, time-to-result, cost, and equipment requirements. Some of these diagnostic kits utilize specific antibodies, while others rely on enzymatic reactions. Most kits generally have a limit of detection of 1 CFU/mL, with some providing results in just a few minutes, while others may take several hours.

Water Samples Analysis

To assess the effectiveness of the sensor in analyzing real samples, a total of 12 different water samples—including tap, bottled mineral, and surface waters, as well as samples taken at various stages of a treatment plant were collected and analyzed. Major physicochemical properties of the water samples including pH, conductivity, salinity, total dissolved solids (TDS), and turbidity—were determined and are reported in Table S2. Initially, two samples—tap water from Tehran's 22nd district and mineral water from the Plour springs—were tasted, revealing no *E. coli O157:H7* contamination, as indicated by the appearing of red emission. Next, these samples were spiked with known concentrations of 10^2, 10^4, and 10^8 CFU/mL; each concentration measured five times by biosensor. Detection was performed by measuring the ratio of green fluorescence from Man-GCDs to red fluorescence from RQDs while illuminating samples with a 440 nm blue-LED. The results agree with the calibration data (Figure 5A,B), indicating that high *E. coli* concentrations produce predominantly green emission, whereas medium and low concentrations yield orange and yellow emissions, respectively. Additionally, both the natural and spiked water samples were compared to results obtained via traditional plate culture methods (Figure 5C,D). The strong agreement between these approaches demonstrates that the biosensor provides accurate and reliable detection of *E. coli O157:H7* contamination, confirming its potential as a rapid and effective analytical tool.

Additionally, ten samples were analyzed: five (Nos. 1−5) from successive stages of a treatment plant and five (Nos. 6−10) surface water samples from various sites in eastern Tehran Province. Two autoclaved, bacteria-free water samples were included as blanks. These samples were analyzed using the sensor, and the results were validated through plate culture methods, as shown in Figures S11. Both testing approaches consistently indicated the presence of *E. coli O157:H7* in all water samples, evidenced by yellow and orange coloration in the test tubes and *E. coli* growth on all plates. Notably, samples 3 and 4 exhibited the highest levels of contamination, while the remaining samples showed similar contamination levels. The strong agreement between the sensor and culture results supports the reliability and accuracy of the sensor method.

These results show that the sensor is applicable across diverse water matrices (Figure S12). Visual appearance ranged from optically clear (samples 1, 8−10) to visibly turbid with suspended particles (samples 3, 4, 6, 7). Moreover, physicochemical parameters also spanned broad ranges according to Table S2: pH ranged from 6.9 to 8.0, electrical conductivity varied between 211.7 and 1073 μS/cm, salinity ranged from 127 to 965 mg/L, TDS ranged from 106 to 804 ppm, and turbidity was between 1 and 20 NTU. Collectively, these data highlight the heterogeneity of the sampled waters and demonstrate that the sensor performs reliably under these varied conditions.

■ CONCLUSIONS

Effective environmental management relies on accurate methods to detect and reduce microbial contaminants in water, which spread disease. Developing detection techniques is crucial. Biosensors enabling visual detection with simple devices are valuable, especially in remote or crisis settings where decisions are needed. However, visual detection often struggles with low analyte concentrations because small signal changes may not produce noticeable color shifts. A ratiometric fluorescence strategy uses multiple emission signals, improving

https://doi.org/10.1021/acs.analchem.5c06000
Anal. Chem. 2026, 98, 818−826

sensitivity and enabling naked-eye semiquantitative detection. This study shows that using a bioinspired receptor, mannose, together with a ratiometric sensing strategy markedly improves *E. coli O157:H7* detection. Mannose binds specifically to *E. coli O157:H7* FimH proteins, offering a cost-effective alternative to antibodies and aptamers and reducing biosensor fabrication costs. Optimizing glycosylation parameters, including mannose loading, was essential to attain a strong initial signal. The ratiometric sensor design uses RQDs as a reference signal and Man-GCDs as a dynamic signal, creating a broad emission range from red to green. This allows visual detection with just a blue LED, as both signals lie in the visible spectrum. In absence of bacteria, red emission dominates; when bacteria are present, labeling with Man-GCDs shifts emission toward yellow, orange, or green in proportion to bacterial concentration. A smartphone with an RGB analyzer can further simplify detection and reduce equipment costs. The method was successfully applied to detect bacterial contamination in various water samples including tap, mineral, surface and groundwater, and samples taken at various stages of a treatment plant. The results closely matched those obtained from traditional plate culture methods but with a significant reduction in analysis time, from 24 h to just 30 min, enabling quicker decision-making in critical situations. Another advantage of this method is that it does not require sophisticated laboratory equipment or trained personnel, making it accessible to individuals with any level of expertise. This ratiometric assay can be extended into a sensor array format for multiplexed identification and discrimination of bacteria with similar surface proteins. By incorporating multiple bioreceptors against other surface proteins, each conjugated to CDs and paired with QD references, an array of sensing elements would generate distinct multivariate "fingerprints" for different strains. These characteristic response patterns can be decoded using chemometric pattern recognition or advanced machine-learning classifiers, enabling high-throughput, sensitive discrimination across closely related bacterial species. Heavy-metal-free fluorophores—such as polymer dots are also promising alternatives as a reference signal.

■ ASSOCIATED CONTENT

Supporting Information

The Supporting Information is available free of charge at https://pubs.acs.org/doi/10.1021/acs.analchem.5c06000.

Experimental Section (chemicals and apparatus, bacterial cultivation and growth, synthesis of green-emitting carbon dots (GCDs), synthesis of red-emitting quantum dots (RQDs), fluorescence microscopy imaging, water samples analysis, and bacterial colony counting on plates); additionally, the document presents result on zeta potential, FTIR analysis, optimization of experimental parameters (pH, component ratios, and incubation time), RGB data, the stability of Man-GCDs and RQDs over temperature, light exposure and time, the photos taken and outcomes of the ratiometric sensor and plate counting for 10 water samples, and tables report comparative study of *E. coli* detection biosensors and the physicochemical properties of the sampled waters (PDF)

■ AUTHOR INFORMATION

Corresponding Author

Saba Ranjbar − *Department of Energy and Environmental Biotechnology, National Institute of Genetic Engineering and Biotechnology (NIGEB), Tehran 14965/161, Iran;* orcid.org/0000-0003-4746-3099; Email: s_ranjbar@nigeb.ac.ir

Authors

Fatemeh Momeni − *Department of Energy and Environmental Biotechnology, National Institute of Genetic Engineering and Biotechnology (NIGEB), Tehran 14965/161, Iran*

Mohammad Amin Farahmand Nejad − *Department of Chemistry, Sharif University of Technology, Tehran 11155-9516, Iran*

Mohammad Reza Hormozi-Nezhad − *Department of Chemistry, Sharif University of Technology, Tehran 11155-9516, Iran;* orcid.org/0000-0002-7472-1850

Complete contact information is available at: https://pubs.acs.org/10.1021/acs.analchem.5c06000

Notes

The authors declare no competing financial interest.

■ ACKNOWLEDGMENTS

Financial support from the National Institute of Genetic Engineering and Biotechnology (NIGEB), Tehran, Iran (Grant No. 862) is appreciated.

■ REFERENCES

(1) Bai, Z.; Xu, X.; Wang, C.; Wang, T.; Sun, C.; Liu, S.; Li, D. A comprehensive review of detection methods for *Escherichia coli* O157:H7. *TrAC, Trends Anal. Chem.* **2022**, *152*, No. 116646.

(2) Jang, J.; Hur, H. G.; Sadowsky, M. J.; Byappanahalli, M.; Yan, T.; Ishii, S. Environmental *Escherichia coli*: ecology and public health implications—a review. *J. Appl. Microbiol.* **2017**, *123* (3), 570−581.

(3) Cotruvo, J. A. 2017 WHO guidelines for drinking water quality: first addendum to the fourth edition. *J. AWWA* **2017**, *109* (7), 44−51.

(4) Odonkor, S. T.; Mahami, T. *Escherichia coli* as a tool for disease risk assessment of drinking water sources. *Int. J. Microbiol.* **2020**, *2020* (1), No. 2534130.

(5) Tack, D. M.; Ray, L.; Griffin, P. M.; et al. Preliminary incidence and trends of infections with pathogens transmitted commonly through food—Foodborne Diseases Active Surveillance Network, 10 US Sites, 2016−2019. *MMWR. Morb. Mortal. Wkly. Rep.* **2020**, *69*, 509−514, DOI: 10.15585/mmwr.mm6917a1.

(6) Shahrokhian, S.; Ranjbar, S. Aptamer immobilization on amino-functionalized metal−organic frameworks: An ultrasensitive platform for the electrochemical diagnostic of *Escherichia coli* O157: H7. *Analyst* **2018**, *143* (13), 3191−3201.

(7) Ranjbar, S.; Nejad, M. A. F.; Parolo, C.; Shahrokhian, S.; Merkoçi, A. Smart chip for visual detection of bacteria using the electrochromic properties of polyaniline. *Anal. Chem.* **2019**, *91* (23), 14960−14966.

(8) Zhou, Q.; Natarajan, B.; Kannan, P. Nanostructured biosensing platforms for the detection of food-and water-borne pathogenic *Escherichia coli*. *Anal. Bioanal. Chem.* **2023**, *415* (16), 3111−3129.

(9) Zhang, J.; Zhou, M.; Li, X.; Fan, Y.; Li, J.; Lu, K.; Wen, H.; Ren, J. Recent advances of fluorescent sensors for bacteria detection-A review. *Talanta* **2023**, *254*, No. 124133.

(10) Fu, W.; Fu, X.; Li, Z.; Liu, Z.; Li, X. Advances in smartphone assisted sensors for on-site detection of food safety based on fluorescence on-off-on mode: A review. *Chem. Eng. J.* **2024**, *489*, No. 151225.

(11) Ashoka, A. H.; Aparin, I. O.; Reisch, A.; Klymchenko, A. S. Brightness of fluorescent organic nanomaterials. *Chem. Soc. Rev.* **2023**, *52* (14), 4525−4548.
(12) Anand, A.; Huang, C.-C.; Lai, J.-Y.; Bano, D.; Pardede, H. I.; Hussain, A.; Saleem, S.; Unnikrishnan, B. Fluorescent carbon dots for labeling of bacteria: mechanism and prospects—a review. *Anal. Bioanal. Chem.* **2024**, *416* (17), 3907−3921.
(13) Huang, Y.; Chen, W.; Chung, J.; Yin, J.; Yoon, J. Recent progress in fluorescent probes for bacteria. *Chem. Soc. Rev.* **2021**, *50* (13), 7725−7744.
(14) Ghirardello, M.; Ramos-Soriano, J.; Galan, M. C. Carbon Dots as an Emergent Class of Sustainable Antifungal Agents. *ACS Nano* **2025**, *19*, 24377−24403, DOI: 10.1021/acsnano.5c03934.
(15) Ghorai, S.; Sen, K.; Dash, P. S. A Review of First-Principles Studies of Carbon Dot Photoluminescence: Implications for Biomedical Applications. *ACS Appl. Nano Mater.* **2024**, *7* (17), 19803−19820.
(16) Ramos-Soriano, J.; Ghirardello, M.; Galan, M. C. Carbon-based glyco-nanoplatforms: towards the next generation of glycan-based multivalent probes. *Chem. Soc. Rev.* **2022**, *51* (24), 9960−9985.
(17) Ajish, J. K.; Kanagare, A. B.; Kumar, K. A.; Subramanian, M.; Ballal, A. D.; Kumar, M. Self-assembled glycobis (acrylamide)-stabilized gold nanoparticles for fluorescent turn-on sensing of lectin and *Escherichia coli*. *ACS Appl. Nano Mater.* **2020**, *3* (2), 1307−1317.
(18) Ranjbar, S.; Astani, N. A.; Atabay, M.; Naseri, N.; Esfandiar, A.; Ejtehadi, M. R. Electrochemical and computational studies of biomimicked Ti3C2Tx MXene-based sensor with multivalent interface. *J. Colloid Interface Sci.* **2022**, *623*, 1063−1074.
(19) Kang, T. W.; Han, J.; Lee, S.; Hwang, I.-J.; Jeon, S.-J.; Ju, J.-M.; Kim, M.-J.; Yang, J.-K.; Jun, B.; Lee, C. H.; et al. 2D transition metal dichalcogenides with glucan multivalency for antibody-free pathogen recognition. *Nat. Commun.* **2018**, *9* (1), No. 2549.
(20) Li, J.; Li, B.; Liu, M. One-step synthesis of mannose-modified polyethyleneimine copolymer particles as fluorescent probes for the detection of *Escherichia coli*. *Sens. Actuators, B* **2019**, *280*, 171−176.
(21) Lai, I. P.-J.; Harroun, S. G.; Chen, S.-Y.; Unnikrishnan, B.; Li, Y.-J.; Huang, C.-C. Solid-state synthesis of self-functional carbon quantum dots for detection of bacteria and tumor cells. *Sens. Actuators, B* **2016**, *228*, 465−470.
(22) Weng, C.-I.; Chang, H.-T.; Lin, C.-H.; Shen, Y.-W.; Unnikrishnan, B.; Li, Y.-J.; Huang, C.-C. One-step synthesis of biofunctional carbon quantum dots for bacterial labeling. *Biosens. Bioelectron.* **2015**, *68*, 1−6.
(23) Sena-Torralba, A.; Torné-Morató, H.; Parolo, C.; Ranjbar, S.; Farahmand Nejad, M. A.; Álvarez-Diduk, R.; Idili, A.; Hormozi-Nezhad, M. R.; Merkoçi, A. A novel ratiometric fluorescent approach for the modulation of the dynamic range of lateral flow immunoassays. *Adv. Mater. Technol.* **2022**, *7* (8), No. 2101450.
(24) Bigdeli, A.; Ghasemi, F.; Abbasi-Moayed, S.; Shahrajabian, M.; Fahimi-Kashani, N.; Jafarinejad, S.; Nejad, M. A. F.; Hormozi-Nezhad, M. R. Ratiometric fluorescent nanoprobes for visual detection: Design principles and recent advances-A review. *Anal. Chim. Acta* **2019**, *1079*, 30−58.
(25) Motamedi-Khozani, R.; Abbasi-Moayed, S.; Hormozi-Nezhad, M. R. Single-Component Double-Emissive Ratiometric Probe: Toward Machine Learning Driven Detection and Discrimination of Neurological Biomarkers. *Anal. Chem.* **2025**, *97* (15), 8248−8257.
(26) Ranjbar, S.; Sarlak, N.; Rashidi, A. Fluorescent-tagged water with carbon dots derived from phenylenediamine as an equipment-free nanotracer for enhanced oil recovery. *J. Colloid Interface Sci.* **2022**, *628*, 43−53.
(27) Koushkestani, M.; Ghasemi, F.; Hormozi-Nezhad, M. R. Ratiometric dual-mode optical sensor array for the identification and differentiation of pesticides in vegetables with mixed plasmonic and fluorescent nanostructures. *ACS Appl. Nano Mater.* **2024**, *7* (3), 2764−2774.
(28) Jiang, K.; Sun, S.; Zhang, L.; Lu, Y.; Wu, A.; Cai, C.; Lin, H. Red, green, and blue luminescence by carbon dots: full-color emission tuning and multicolor cellular imaging. *Angew. Chem.* **2015**, *127* (18), 5450−5453.
(29) Jiang, K.; Feng, X.; Gao, X.; Wang, Y.; Cai, C.; Li, Z.; Lin, H. Preparation of multicolor photoluminescent carbon dots by tuning surface states. *Nanomaterials* **2019**, *9* (4), No. 529.
(30) Chung, Y. J.; Lee, B. I.; Park, C. B. Multifunctional carbon dots as a therapeutic nanoagent for modulating Cu (ii)-mediated β-amyloid aggregation. *Nanoscale* **2019**, *11* (13), 6297−6306.
(31) Borse, V.; Kashikar, A.; Srivastava, R. Fluorescence stability of mercaptopropionic acid capped cadmium telluride quantum dots in various biochemical buffers. *J. Nanosci. Nanotechnol.* **2018**, *18* (4), 2582−2591.
(32) Miao, X.; Qu, D.; Yang, D.; Nie, B.; Zhao, Y.; Fan, H.; Sun, Z. Synthesis of carbon dots with multiple color emission by controlled graphitization and surface functionalization. *Adv. Mater.* **2018**, *30* (1), No. 1704740.
(33) Sato, R.; Iso, Y.; Isobe, T. Fluorescence solvatochromism of carbon dot dispersions prepared from phenylenediamine and optimization of red emission. *Langmuir* **2019**, *35* (47), 15257−15266.
(34) Chen, C.-L.; Dudek, A.; Liang, Y.-H.; Janapatla, R. P.; Lee, H.-Y.; Hsu, L.; Kuo, H.-Y.; Chiu, C.-H. d-mannose-sensitive pilus of Acinetobacter baumannii is linked to biofilm formation and adherence onto respiratory tract epithelial cells. *J. Microbiol. Immunol. Infect.* **2022**, *55* (1), 69−79.
(35) Zhao, Y.; Li, Y.; Zhang, P.; Yan, Z.; Zhou, Y.; Du, Y.; Qu, C.; Song, Y.; Zhou, D.; Qu, S.; Yang, R. Cell-based fluorescent microsphere incorporated with carbon dots as a sensitive immunosensor for the rapid detection of *Escherichia coli* O157 in milk. *Biosens. Bioelectron.* **2021**, *179*, No. 113057.
(36) Wang, S.; Liang, N.; Hu, X.; Li, W.; Guo, Z.; Zhang, X.; Huang, X.; Li, Z.; Zou, X.; Shi, J. Carbon dots and covalent organic frameworks based FRET immunosensor for sensitive detection of *Escherichia coli* O157: H7. *Food Chem.* **2024**, *447*, No. 138663.
(37) Zhang, H.; Liu, M.; Liu, Y.; Xiao, J.; Ren, Y.; Gao, X. Portable real-time determination of *Escherichia coli* O157: H7 and Staphylococcus aureus based on smartphones and hydrogels. *Spectrochim. Acta, Part A* **2025**, *325*, No. 125119.
(38) Bai, X.; Ga, L.; Du, Y.; Ai, J. Carbon quantum dot-based label-free fluorescent biosensor to detect *E. coli*. *IEEE Sens. J.* **2024**, *24* (16), 25284−25290.
(39) Bhatt, D.; Singh, S.; Singhal, N.; Bhardwaj, N.; Deep, A. Glyco-conjugated metal−organic framework biosensor for fluorescent detection of bacteria. *Anal. Bioanal. Chem.* **2023**, *415* (4), 659−667.
(40) Wu, D.; Wang, D.; Ye, X.; Yuan, K.; Xie, Y.; Li, B.; Huang, C.; Kuang, T.; Yu, Z.; Chen, Z. Fluorescence detection of *Escherichia coli* on mannose modified ZnTe quantum dots. *Chin. Chem. Lett.* **2020**, *31* (6), 1504−1507.

https://doi.org/10.1021/acs.analchem.5c06000
Anal. Chem. 2026, 98, 818−826